Journal of Materials Chemistry

Cite this: J. Mater. Chem., 2012, 22, 16382

www.rsc.org/materials

PAPER

The biaxial lamello-columnar liquid crystalline structure of a tetrathiafulvalene sanidic molecule

Dae-Yoon Kim,†[a] Lei Wang,†[b] Yan Cao,[c] Xinfei Yu,[c] Stephen Z. D. Cheng,[c] Shiao-Wei Kuo,[d] Dae-Hyun Song,[a] Seung Hee Lee,[a] Myong-Hoon Lee*[a] and Kwang-Un Jeong*[a]

Received 3rd April 2012, Accepted 22nd June 2012
DOI: 10.1039/c2jm32070c

A macroscopically oriented lamello-columnar mesophase was obtained from a newly designed and synthesized symmetric tetrathiafulvalene-based molecule (symTTF11) containing four flexible alkyl chains chemically attached to the periphery of TTF mesogens (L. Wang, *et al.*, *J. Mater. Chem.*, 2011, **21**, 60), and its phase behaviors and physical properties were investigated by the combined experimental techniques. Based on the experimental results and structure analyses, it was revealed that there are two ordered columnar phases below the isotropic phase: a columnar crystalline phase (Col_K) and a columnar smectic liquid crystal phase (Col_L). From two-dimensional wide angle X-ray diffraction patterns of the macroscopically oriented samples, phase structures of Col_K and Col_L were identified and their biaxial molecular packing structures were also proposed. Since the assembled symTTF11 columns were well organized in the ordered layer structures over a macroscopic domain, symTTF11 exhibited a good charge carrier mobility in the Col_L phase.

Introduction

Molecular self-assembly is a spontaneous organization process achieved by the programmed physical molecular interactions, such as hydrogen bonding, electrostatic (ion–ion, ion–dipole, and dipole–dipole) interaction, π-orbital overlapping, van der Waals interaction, and the hydrophobic–hydrophilic effect.[1–5] Especially, self-assembled discotic liquid crystal (LC) molecules have attracted a lot of attention as promising charge-transfer organic candidates. The excellent electrical/photo conductivity along the long axis of discotic columns constructed by intermolecular π–π interaction and nanophase separation plays a very important role in practical applications, such as field-effect transistors, electroluminescent displays, and photovoltaic cells.[6–31] In order to maximize their physical properties, it is essential to control their molecular packing structure and morphology on the different length scales from sub-nanometer to micrometer since their physical properties strongly depend on the nature of molecular self-assembly and organization.[19–22]

By attaching flexible alkyl chains at the periphery of board-shaped aromatic LC mesogens, solution-processable columnar and smectic LCs (so-called "lamello-columnar LCs", abbreviated as Col_L) have been reported in recent years.[23–27] The Col_L LC phases show good charge carrier mobilities in their mesophases, in which the self-assembled two-dimensional (2D) columns are well organized in the ordered layer structures over a macroscopic domain.[28,29] Due to the restricted rotation of the molecules within the layers, Col_L additionally exhibits peculiar physical properties such as optical biaxiality and macroscopic polar order.[10]

From the perspective of developing new types of Col_L LC materials, four flexible alkyl chains are chemically attached to the periphery of a new tetrathiafulvalene (TTF) board-shaped mesogen fused with two naphthalene rings.[16] TTF derivatives are good electron donors and their planar geometries can promote intermolecular π–π interactions, resulting either in self-assembled columns or in layers.[30–41] Ester linkage is purposely selected to increase the air/light stability of the electron-rich TTF mesogen by decreasing the highest occupied molecular orbital (HOMO) levels of TTF.[42,43] Instability of TTF has been one of the main drawbacks of TTF-based molecules for the optoelectronic applications.[16,44] When the number of carbon atoms in an alkyl chain is 11, the TTF-based molecule is abbreviated as symTTF11, as illustrated in Fig. 1a. The phase transitions of symTTF11 are studied by combined techniques of differential scanning calorimetry (DSC), 1D wide angle X-ray diffraction (WAXD), cross-polarized optical microscopy (POM), and solid-state carbon-13 (^{13}C) nuclear magnetic resonance (NMR) experiments. The structure, molecular packing symmetry and

[a]*Department of Polymer-Nano Science and Technology, Department of Flexible and Printable Electronics, Department of BIN Fusion Technology, Chonbuk National University, Jeonju, 561-756, Korea. E-mail: kujeong@jbnu.ac.kr; mhlee2@jbnu.ac.kr; Fax: +82 63 270 2341; Tel: +82 63 270 4633*
[b]*National Centre for Nanoscience and Technology, Beijing 100190, China*
[c]*College of Polymer Science and Engineering, The University of Akron, Akron, Ohio 44325, USA*
[d]*Department of Materials Science and Optoelectronic Engineering, National Sun Yat-Sen University, Kaohsiung 804, Taiwan*
† These authors contributed equally to this work.

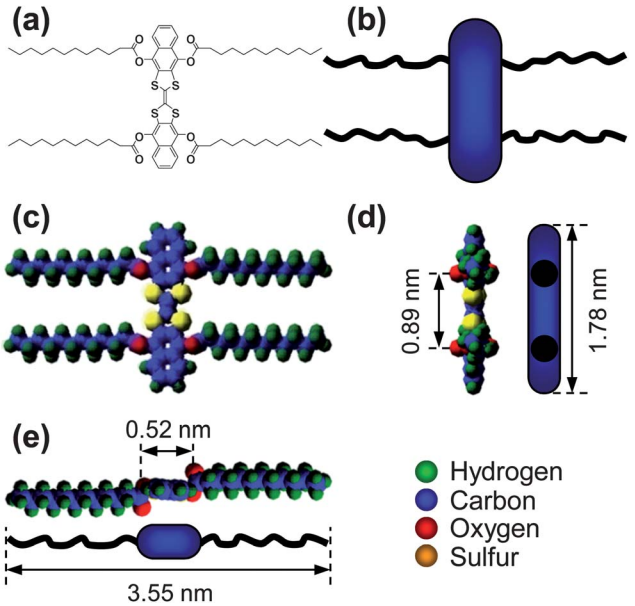

Fig. 1 (a) Chemical structure and (b) schematic illustration of symTTF11 molecule. Calculated geometric dimensions of symTTF11 molecule in the views from (c) front, (d) side and (e) head.

morphology are first identified using 2D WAXD from oriented films and their results are further confirmed by selected area electron diffractions (SAED) from transmission electron microscopy (TEM). Since the self-assembled symTTF11 columns in the LC phase are well organized over a macroscopic domain, symTTF11 in the LC phase shows a good charge carrier mobility.[16]

Results and discussion

Utilizing Cerius^2 (Version 4.6, Accelrys) computer simulation software, molecular dimensions and global equilibrium conformations of symTTF11 in the isolated gas phase are first estimated under the COMPASS force field. The results are represented in Fig. 1c–e. The energy-minimized symTTF11 mesogen maintains a planar conformation and its calculated length and width are 1.78 and 0.52 nm, respectively, while the alkyl chains attached to the sides of the symTTF11 mesogen are separated by a distance of 0.89 nm, as represented in Fig. 1d and e. Based on the assumption of the all-*trans* conformation in the alkyl chains, the length of symTTF11 perpendicular to the long axis of symTTF11 mesogen is 3.55 nm. Schematic illustrations of symTTF11 are also represented in Fig. 1.

To detect thermal transitions of symTTF11 and to obtain their quantitative thermodynamic properties, DSC experiments are conducted during cooling and subsequent heating processes at 1.0 °C min^{-1} scanning rate and their results are shown in Fig. 2. Two first-order thermal transitions are detected during cooling and subsequent heating processes. The high temperature transition appears at 172 °C with a heat of transition of −28 J g^{-1} (−33.5 kJ mol^{-1}) which is independent of the cooling rate. The independence of the exothermic transition temperature and its heat of transition indicate that the high temperature transition takes place close to the thermodynamic equilibrium. It is worth noting that

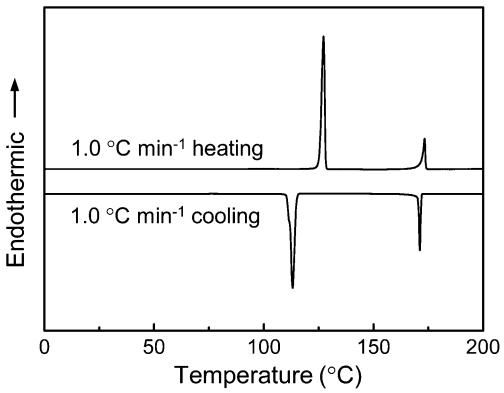

Fig. 2 A set of DSC cooling and subsequent heating thermal diagrams of symTTF11 at 1.0 °C min^{-1}.

this behaviour is often observed from an isotropic melt (I) to a LC phase.[45–48] On the other hand, the onset temperature and the heat of transition of the low temperature exothermic transition exhibit the supercooling effect during a crystallization process.[49–51] The subsequent heating diagram immediately following the cooling process shows two endothermic transitions (at 123 °C with 147 kJ mol^{-1} and 172 °C with 33.5 kJ mol^{-1}), which correspond to the two exothermic transitions found (at 114 °C and 172 °C) during the previous cooling process. Although DSC experiments are sensitive to heat absorption and release events at thermal transitions and can give quantitative thermodynamic properties, this technique does not usually provide direct information of ordered structural evolutions associated with the transitions. Therefore,

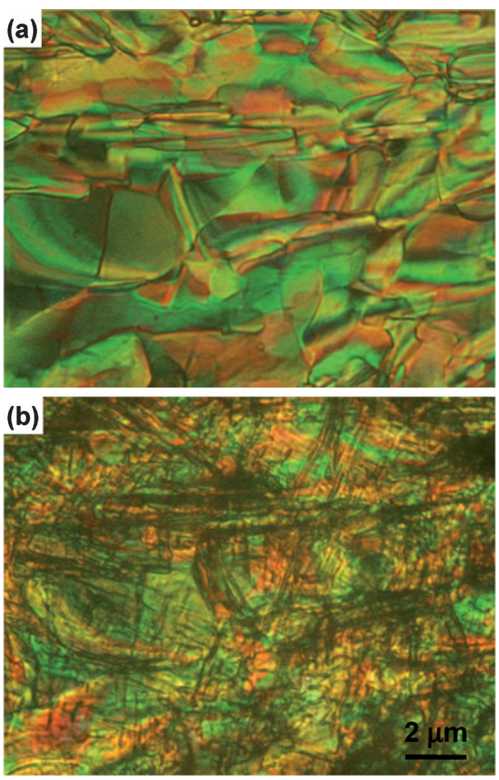

Fig. 3 POM images of symTTF11 at (a) 150 °C and (b) 25 °C.

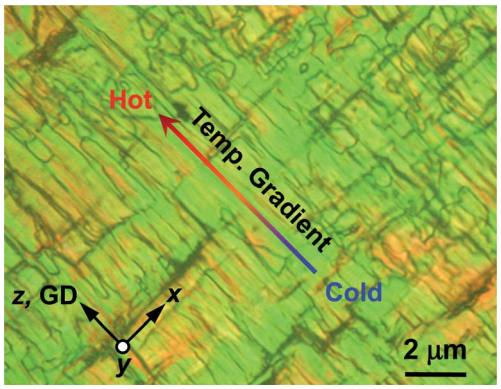

Fig. 4 POM image of the oriented symTTF11 crystal grown on the temperature gradient surface between 200 °C and 25 °C. Here, GD means the growth direction and *xyz* Cartesian coordinate represents the symTTF11 sample geometry in a real space.

the formations of these two ordered phases are monitored under cross-polarized optical microscopy (POM), as shown in Fig. 3. The photograph taken at 150 °C (Fig. 3a) shows a mosaic texture.[50,52] Further decreasing the temperature to 25 °C results in strong birefringent aggregates with cracks (Fig. 3b), which often occurs due to the anisotropic volume shrinkage during the crystallization process. Based on the POM results combined with those of DSC, it is realized that there are two ordered phases below the isotropization temperature (172 °C): one is a LC phase and the other is a crystalline phase.

To obtain the detailed structural and symmetry information in each of these two ordered phases, 2D WAXD experiments from oriented symTTF11 samples must be conducted. Macroscopically oriented symTTF11 crystals for 2D WAXD experiments are prepared on the temperature gradient surface between 200 and 25 °C. The POM texture of the oriented symTTF11 crystal taken at 25 °C is represented in Fig. 4. Note that cracks are generated mainly along the *xy*- and *yz*-planes in the *xyz* Cartesian coordinate of specimens, which is closely related to symmetry and molecular packing of symTTF11. Here, GD represents the fast growth direction of symTTF11 crystal.

A series of 2D WAXD patterns for the oriented symTTF11 crystals is obtained when the incident X-ray beam directions are normal to the [001] (Fig. 5a), the [010] (Fig. 5b) and the [100] (Fig. 5c) zones, respectively. In these patterns, diffraction information about symTTF11 molecular arrangements appears on two different length scales. One is on the nanometer length scale in the low 2θ-angle region between 1.5° and 11°, in which the self-organization information of self-assembled TTF columns can be obtained. Diffractions on the sub-nanometer length scale between 11° and 30° can provide information about the molecular packing structures inside of columns as well as about the molecular correlations between neighbouring columns. Diffraction arc positions and widths in Fig. 5a–c are calibrated based on the isotropic diffraction ring of silicon power crystal at $2\theta = 28.466°$ ($d = 0.314$ nm). Based on these 2D WAXD patterns (Fig. 5a–c), it is realized that macroscopically oriented symTTF11 crystals are obtained on the millimeter length scale *via* the organization of symTTF11 on the temperature gradient surface (Fig. 4 and 5d). When the X-ray beam is irradiated parallel to the growth direction (GD, *z*-axis), 2D WAXD on the [001] zone is obtained and shown in Fig. 5a. On the equator assigned as the *b**-axis, a pair of diffraction arcs appears at $2\theta = 2.22°$ ($d = 3.98$ nm) with its high order diffractions at $2\theta = 4.45°$, 8.91°, 13.38° and 17.87°, which are assigned as (010), (020), (040), (060) and (080), respectively. There is no diffraction observed on the meridian (the *a*-axis), but two pairs of diffractions in the first

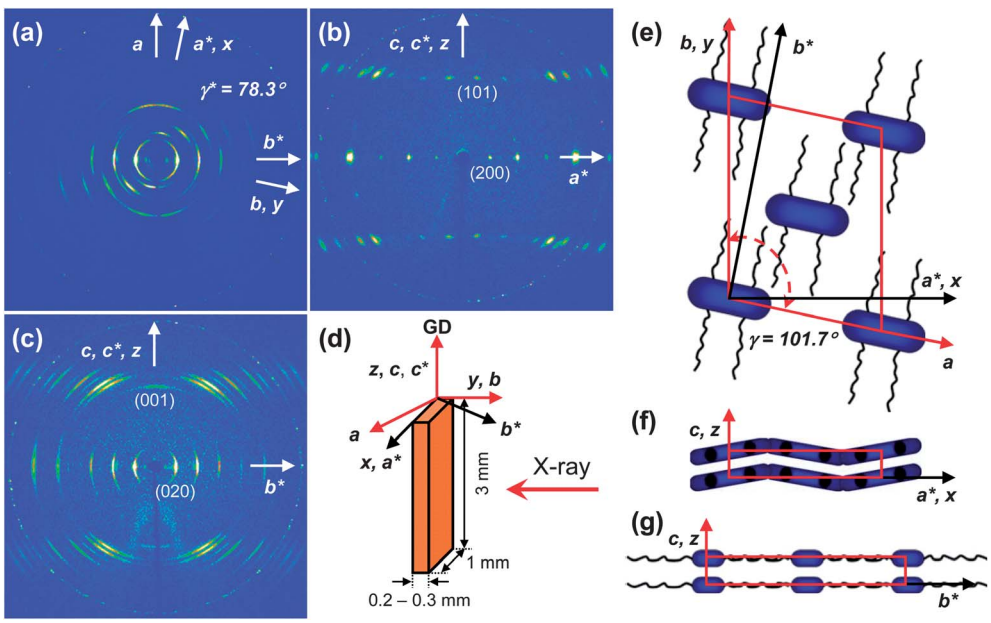

Fig. 5 2D WAXD patterns of the crystalline phase (Col_K) of symTTF11 at 25 °C: (a) the [001], (b) the [010] and (c) the [100] zones, respectively. Schematic illustrations of (d) symTTF11 specimen and molecular packing models of symTTF11 on (e) the [001], (f) the [010] and (g) the [100] zones, respectively. Here, GD means the growth direction, and *xyz*, *abc* and *a***b***c** are Cartesian coordinates representing sample and unit cell geometries in real and reciprocal spaces, respectively.

Table 1 Experimental and calculated crystallographic parameters of the columnar crystalline phase (Col_K) of symTTF11

	2θ (deg)		d-spacing (nm)	
hkl	Expt[a]	Calc.[b]	Expt[a]	Calc.[b]
010	2.22	2.22	3.98	3.97
020	4.45	4.45	1.99	1.99
040	8.90	8.91	0.99	0.99
060	13.40	13.38	0.66	0.66
080	17.85	17.87	0.50	0.50
200	5.75	5.73	1.54	1.54
$\bar{2}20$	7.95	7.94	1.11	1.11
$\bar{2}40$	9.60	9.57	0.92	0.92
400	11.50	11.48	0.77	0.77
420	13.15	13.13	0.77	0.67
600	17.25	17.25	0.51	0.51
620	18.70	18.69	0.47	0.47
001	16.60	16.60	0.53	0.53
031	17.90	17.91	0.50	0.50
051	20.05	20.04	0.44	0.44
101	16.85	16.85	0.53	0.53
201	17.60	17.58	0.50	0.50
301	18.75	18.73	0.47	0.47
401	20.25	20.23	0.44	0.44
501	22.00	22.02	0.40	0.40
601	24.05	24.03	0.37	0.37
302	34.70	34.71	0.26	0.26
502	36.70	36.68	0.24	0.25
602	38.00	37.98	0.24	0.24

[a] The accuracy of the experimental data is ±0.005 nm. [b] The calculated data listed are based on the columnar crystalline (Col_K) monoclinic unit cell with a = 3.149 nm, b = 4.056 nm, c = 0.534 nm, $\alpha = \beta$ = 90.0° and γ = 101.7°.

and third quadrants are detected at $2\theta = 5.73°$ ($d = 1.54$ nm) and 11.48° (d = 0.77 nm), which are 11.7° out of the meridian direction (assigned as the a*-axis). These diffractions should be assigned as (200) and (400) based on the extinct law of the diffraction principle.[45,46] This Miller index assignment is strongly supported by the (h01) diffractions on the [010] zone 2D WAXD pattern (Fig. 5b) which is obtained by exposing the X-ray beam along the b*-axis (11.7° away from the y-axis). As shown in Fig. 5b, the (h01) diffractions with the odd numbers of h are detected. When the X-ray beam is along the x-axis (parallel to the a*-axis), the [100] 2D WAXD pattern is obtained as shown in Fig. 5c. The diffraction pattern on the equator is identical to that of the [001] 2D WAXD pattern and the meridian direction is identified as the c*-axis. From these 2D WAXD results, it is realized that this crystal possesses a monoclinic lattice with a = 3.149 nm, b = 4.056 nm, c = 0.534 nm, $\alpha = \beta = 90.0°$ and γ = 101.7°. Table 1 lists the experimentally observed and the calculated d-spacings based on this unit cell lattice. With four symTTF11 molecules in one unit cell, its calculated crystallographic density is 1.19 g cm^{-3}. The experimentally observed density is 1.17 g cm^{-3}, which fits well with the calculated one. Therefore, this phase is identified as a monoclinic columnar crystalline phase and abbreviated as Col_K.

Based on the 2D WAXD patterns and structure analyses, molecular packing structures in the unit cell lattice are proposed, as shown in Fig. 5e–g. As schematically illustrated in Fig. 5e, the in-plane of symTTF11 is perpendicular to the GD of crystal and the long axis of symTTF11 mesogens is more or less parallel to the a-axis so that alkyl chains attached to the periphery of the mesogens are parallel to the b*-axis. These alkyl chains are interdigitated with neighbouring ones and crystallized. This can be explained by the asymmetric diffraction patterns observed along the [001] zone. Since the (101) diffraction at 2θ = 16.85° (d = 0.526 nm, the distance of π–π interaction) is ±10° away from the meridian direction, the normal axis of symTTF11 molecules is ±10° tilted from the long axis of the face-to-face assembled columns (GD) and packed along the x-axis with an anticlinically tilted fashion. The interdigitated alkyl chains represented in Fig. 5g is also supported by comparing the molecular geometric dimensions of symTTF11 (the longest length = 3.55 nm, Fig. 1e) and the unit cell dimension (d_{010} = 3.97 nm). The structural determination and proposed molecular packing

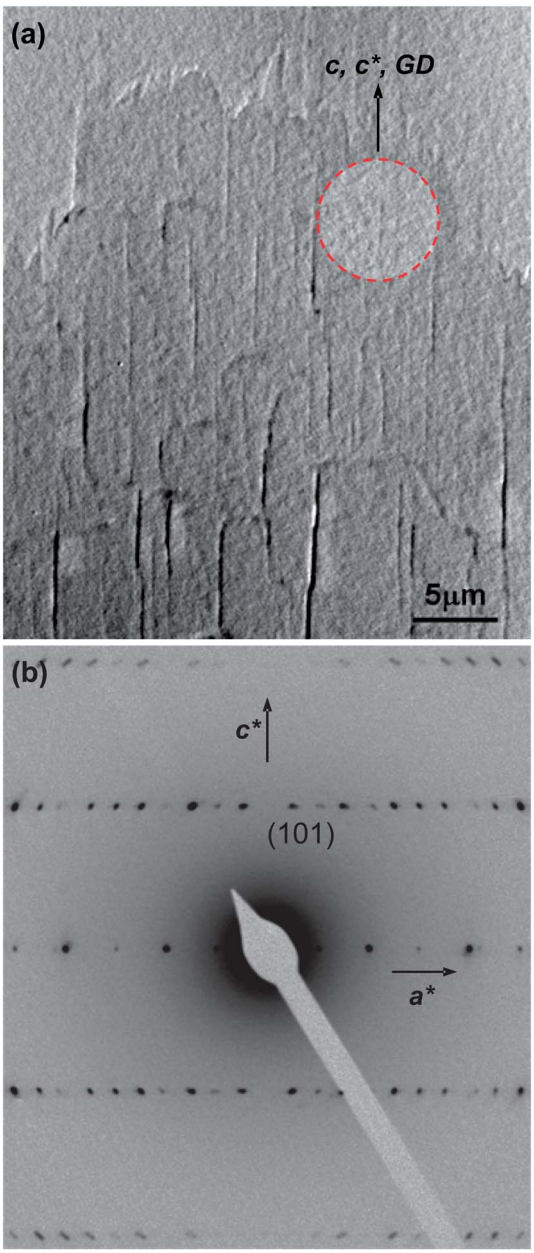

Fig. 6 (a) Bright-field TEM morphology of symTTF11 in the Col_K phase and (b) SAED pattern from the circled area of the bright-field TEM morphology in (a).

structure of symTTF11 are also supported by SAED (Fig. 6b) obtained from the Col_K single crystal (Fig. 6a). SAED is obtained without any sample tilting and its result is well matched with the [010] 2D WAXD pattern (Fig. 5b). High order (h01) and (h02) diffractions detected on the SAED pattern additionally support the molecular packing symmetry represented in Fig. 5e–g.

The molecular packing structure of the mesophase between 123 °C and 172 °C is also identified from the [001], the [010] and the [100] 2D WAXD patterns, as shown in Fig. 7a–c, respectively. From these 2D WAXD patterns, it is realized that the 2D WAXD patterns are all symmetric and molecular orientations are not much changed. When the X-ray beam is irradiated parallel to the GD (Fig. 7a) or the x-axis (Fig. 7c) at 150 °C, a scattering halo appears at $2\theta = \sim 21°$ ($d = 0.423$ nm), which is attributed to the packing of the alkyl tails in the high-temperature phase. In order to confirm this explanation, the solid-state ^{13}C NMR spectra with Cross Polarization/Magic Angle Spinning/Dipolar Decoupling (CP/MAS/DD) (Fig. 8a) and Bloch decay (Fig. 8b) are acquired at different temperatures to selectively investigate the rigid and mobile components, respectively. As shown in Fig. 8a, the solid-state ^{13}C NMR spectra with CP/MAS/DD are not changed in the chemical shift from 100 to 200 ppm. This result indicates the fact that the assembled TTF mesogens in the ordered states are fairly rigid. The chemical shift at 33.5 ppm in the Block decay ^{13}C solid-state NMR spectra of symTTF11 (Fig. 8b) represents the methylene carbon atoms in the long *trans* zigzag segments of the alkyl tails, while the chemical shift at 30.5 ppm corresponds to the carbon atoms in the disordered, statistically distributed *trans* and *gauche* conformations.[53–59] In the Col_K phase, more than 90% of CH_2 carbon atoms are in the relatively long *trans* zigzag conformations, while the percentage of *trans* conformations in the I phase is below 30%. By increasing the temperature to the mesophase, the *trans* conformation of CH_2 carbons decreases to the level of 65%, implying there is some residual amount of ordered alkyl tails. On the equator of the [001] and the [100] 2D WAXD, a set of the (0h0) diffractions is detected at $2\theta = 3.33°$ ($d = 2.65$ nm), 6.67° ($d = 1.33$ nm), 10.01° ($d = 0.88$ nm) and 10.36° ($d = 0.66$ nm). Since the diffused (031) and (051) diffractions are detected at $2\theta = 17.47°$ ($d = 0.51$ nm) and 18.72° ($d = 0.47$ nm) on the [100] zone of the 2D WAXD pattern (Fig. 7c), the h values in the (0h0) diffractions should be even numbers. On the meridian of the [001] 2D WAXD pattern (Fig. 7a), a pair of weak diffraction appears at $2\theta = 5.61°$ ($d = 1.58$ nm), which is assigned to be (200). This assignment is confirmed from the series of (h0l) diffractions on the [010] 2D WAXD pattern (Fig. 7b). In contrast to the [001] and the [100] 2D WAXD patterns, the [010] 2D WAXD pattern seems to represent highly ordered crystals. These 2D WAXD patterns at 150 °C indicate that symTTF11 mesogens still remain in the highly ordered state while the alkyl chains chemically attached to the peripheries of symTTF11 mesogens are in the somewhat disordered molten state. Based on the [001], the [010] and the [100] 2D WAXD patterns and structure analyses, it is identified that this mesophase consists of an orthorhombic unit cell with dimensions of $a = 3.150$ nm, $b = 5.300$ nm and $c = 0.530$ nm. The molecular packing structures in the unit cell lattice are proposed as shown in Fig. 7e–g. Table 2 lists the experimentally observed and the calculated d-spacings based on this unit cell lattice. With four symTTF11 molecules in one unit cell, it is calculated that crystallographic density is 0.90 g cm^{-3}, which is lower than that of Col_K. Therefore, this phase is identified as a Col_L mesophase.

Comparing to unit cell dimensions of the Col_K, the b-axis of Col_L is expanded about 30% while γ-angle is reduced from 101.7° to 90.0°. This result can be explained by the fact that the alkyl

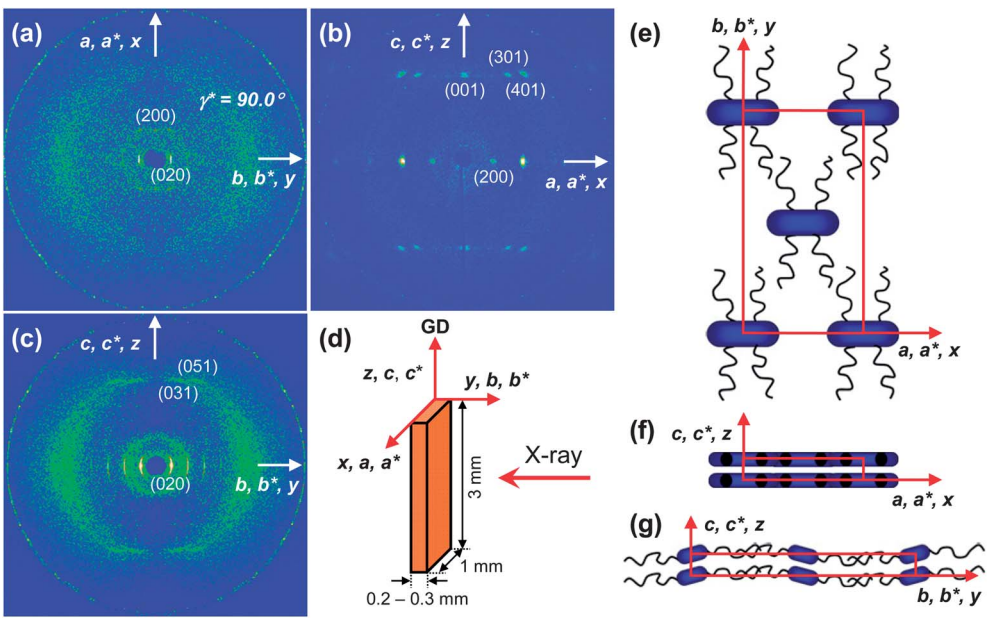

Fig. 7 2D WAXD patterns of the highly ordered columnar smectic LC phase (Col_L) of symTTF11 at 150 °C: (a) the [001], (b) the [010] and (c) the [100] zones, respectively. Schematic illustrations of (d) symTTF11 specimen and molecular packing models of symTTF11 on (e) the [001], (f) the [010] and (g) the [100] zones, respectively. Here, GD means the growth direction, and xyz, abc and $a^*b^*c^*$ are Cartesian coordinates representing sample and unit cell geometries in real and reciprocal spaces, respectively.

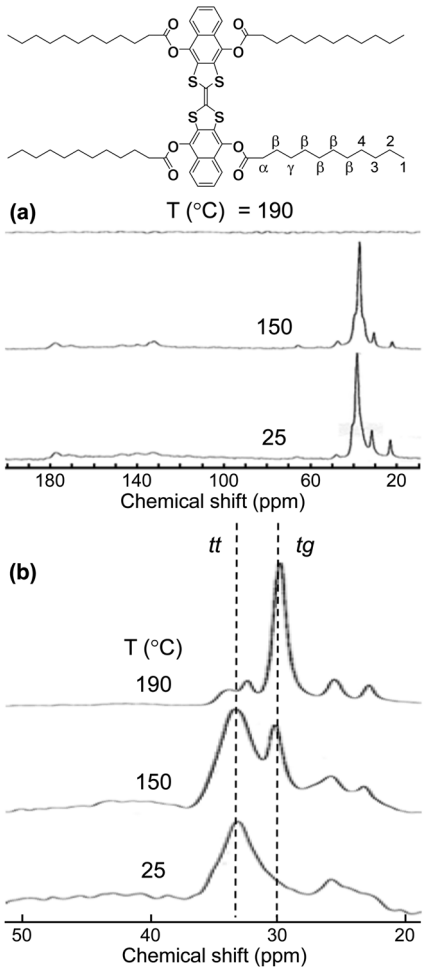

Fig. 8 Sets of solid-state ^{13}C NMR spectra of symTTF11 during cooling between 190 °C and 25 °C with (a) CP/MAS/DD and (b) Bloch decay methods.

chains are interdigitated during the crystallization process so that the macroscopic cracks are generated along the GD (Fig. 4). However, the *c*-axes of Col_K and Col_L are almost identical, which means that the π–π interactions between symTTF11 mesogens occurred in all the ordered phases. This structural and morphological observation can be directly associated with the electric property of symTTF11-based thin film transistor (TFT).[16] The charge mobility of symTTF11 in the Col_L phase is around 10^{-5} cm^2 V s^{-1}, yet the mobility suddenly decreases to 10^{-7} cm^2 V s^{-1} after the crystallization process.[16] This two-order of magnitude decrease must be originated from the generation of macroscopic cracks during the crystallization process. Based on our experimental results, it can be concluded that the high-temperature transition at 172 °C is mainly attributed to the face-to-face assembly of symTTF11 to the rectangular columns followed by the self-organization of the assembled columns to the Col_L phase. Here, the driving forces of the I–Col_L transition are attributed to the π–π interaction between symTTF11 mesogens and nanophase separation between rigid symTTF11 mesogen and flexible alkyl chains. Based on the solid-state ^{13}C NMR combined with 2D WAXD results, it is known that the low-temperature transition at 114 °C is mainly originated from the crystallization of alkyl chains.

Table 2 Experimental and calculated crystallographic parameters of the lamello-columnar LC phase (Col_L) of symTTF11

	2θ (deg)		*d*-spacing (nm)	
hkl	Expt[a]	Calc.[b]	Expt[a]	Calc.[b]
020	3.33	3.33	2.65	2.65
040	6.70	6.67	1.32	1.33
060	10.00	10.01	0.89	0.88
080	13.35	13.36	0.66	0.66
200	5.60	5.61	1.58	1.58
400	11.25	11.24	0.79	0.79
600	16.90	16.89	0.52	0.53
001	16.75	16.73	0.53	0.53
031	17.50	17.47	0.51	0.51
051	18.70	18.72	0.48	0.47
101	16.95	16.96	0.52	0.52
201	17.65	17.66	0.50	0.50
301	18.75	18.75	0.47	0.47
401	20.20	20.20	0.44	0.44

[a] The accuracy of the experimental data is ±0.005 nm. [b] The calculated data listed are based on the lamello-columnar LC (Col_L) orthorhombic unit cell with $a = 3.150$ nm, $b = 5.300$ nm and $c = 0.530$ nm.

Experimental

Materials and sample preparations

A series of symmetric TTF-based LC molecules was newly designed and synthesized.[16] This series of TTF derivatives were purified by column chromatography several times before examination. Their chemical structure and purity were confirmed by proton (^1H) NMR, carbon-13 (^{13}C) NMR, Fourier-transform infrared spectroscopy (FT-IR), elemental analyses and high-resolution mass spectrometry, which can be found in ref. 16. One of this series of symmetric TTF molecules (symTTF11) was analyzed as a representative sample of the series. The molecular weight of symTTF11 was 1199 g mol^{-1}. The molecular dimensions and minimal energy geometry of symTTF11 in the isolated gas phase were estimated by utilizing Cerius^2 (Version 4.6) computer simulation software from Accelrys.

To determine various phase structures of symTTF11, oriented samples for 2D WAXD experiments were first obtained by self-organizations on thermal gradient hot plates and then thermally treated at different temperatures. A typical sample thickness was about 0.2 mm. The samples prepared for cross-polarized optical microscopy (POM) had a typical thickness of 10 μm, and they were melt-processed between two bare cover glasses. The powder samples were used for solid-state ^{13}C NMR. Thin film samples prepared for TEM *via* solution casting from a 0.05% (w/v) chloroform solution onto carbon-coated mica had a thickness of 50–150 nm. After evaporation of solvent, the films were floated on a water surface and recovered using the TEM copper grids. To improve the contrast of the TEM image, platinum shadowing was applied before observation.

Equipment and experiments

The thermal behavior of the phase transitions was studied using a Perkin-Elmer PYRIS Diamond DSC with an Intracooler 2P apparatus. The temperatures and heat flows were calibrated using material standards at cooling and heating rates ranging

from 1.0 to 40 °C min^{-1}. Heating experiments always preceded the cooling experiments in order to eliminate previous thermal histories, and the cooling and heating rates were always kept identical. The transition temperatures were determined by measuring the onset temperatures from both the cooling and heating scans at different rates.

The oriented 2D WAXD patterns were obtained using a Rigaku X-ray imaging system with an 18 kW rotating anode X-ray generator. The diffraction peak positions and widths were calibrated with silicon crystals in the high 2θ-angle region (>15°) and silver behenate in the low 2θ-angle region. A hot stage was also used to obtain diffraction peaks from the ordered structures at elevated temperatures. A 30 min exposure time was required for a high-quality pattern. In 2D WAXD experiments, background scattering was subtracted from the sample scans.

The conformations of the alkyl chain in symTTF11 at different temperatures were also studied using solid-state ^{13}C NMR spectroscopy (Chemagnetics CMX 200) operating at 201.13 and 50.78 MHz for ^{1}H and ^{13}C nuclei, respectively. The samples were spun in nitrogen gas at 4.5 kHz at the magic angle. The magic angle was optimized by the intensity calibration of the aromatic carbon resonance of hexamethylbenzene. The ^{13}C NMR spectra with CP/MAS/DD were acquired to selectively investigate the rigid components, and the Bloch decay spectra with MAS/DD were used to particularly study the mobile components. The CP contact time was 1 ms, while the recycle time of the pulse was 5 s. Each spectrum consisted of an accumulation of 500 scans. The temperature of the solid-state ^{13}C NMR experiment was controlled using a REX-F900 VT unit.

Bright-field TEM images (FEI Tacnai 12) were obtained to examine the film morphology on the nanometer length scale using an accelerating voltage of 120 kV. The camera length for SAED was set at 3.0 m and the calibration of the SAED spacing smaller than 0.384 nm was carried out using evaporated thallous chloride, which has a largest first-order spacing diffraction of 0.384 nm. Spacing values larger than 0.384 nm were calibrated by doubling the *d*-spacing values of the first-order diffractions.

Optical textures of the ordered phases at different temperatures were observed with POM (Nikon ECLIPSE E600POL) coupled with a LINKAM LTS 350 heating stage in order to investigate morphology on the micrometer scale. The Cerius^2 (Version 4.6) simulation software from Accelrys was used to calculate the global equilibrium conformation of the symTTF11 compound in the isolated gas phase utilizing the COMPASS force field. Overlapped carbon peaks in solid-state ^{13}C NMR were resolved using the PeakFit peak separation program from Jandel Scientific. Lorentzian functions were used to obtain the best reasonable fit.

Conclusions

Phase behaviors and structures of a board-shaped TTF-based LC molecule (symTTF11) were investigated by the combined techniques of DSC, POM, TEM, 2D WAXD, SAED and solid-state ^{13}C NMR. Based on the experimental results and structure analyses, it was revealed that there are two column-based phases below I phase: a columnar crystalline phase (Col_K) and a columnar smectic LC phase (Col_L). From 2D WAXD and SAED patterns, phase structures of Col_K and Col_L were identified and their molecular packing structures were proposed. Since the assembled symTTF11 columns were well organized in the ordered layer structures over a macroscopic domain, symTTF11 showed a good charge carrier mobility in the Col_L phase, which was about two-order of magnitude faster than that in the Col_K phase. Due to the restricted rotation of the molecules within the layers, the Col_L phase of symTTF11 may exhibit unique physical properties such as biaxiality and macroscopic polar order which are under investigations.

Acknowledgements

This work was mainly supported by Basic Science Research Program (NRF2011-0004900), Converging Research Center Program (2011K000776) and Human Resource Training Project for Regional Innovation funded by the Ministry of Education, Science Technology of Korea.

Notes and references

1 G. Sun and C.-C. Chu, *ACS Nano*, 2009, **3**, 1176.
2 M. J. Molla and S. Ghosh, *Chem. Mater.*, 2011, **23**, 95.
3 J.-R. Gong, S.-B. Lei, L.-J. Wan, G.-J. Deng, Q.-H. Fan and C.-L. Bai, *Chem. Mater.*, 2003, **15**, 3098.
4 X. Dou, G. Li and H. Lei, *Nano Lett.*, 2008, **8**, 1286.
5 H. C. Zeng, *J. Mater. Chem.*, 2011, **21**, 7511.
6 D. Adam, P. Schuhmacher, J. Simmerer, L. Haussling, K. Siemensmeyer, K. Etzbach, H. Ringsdorf and D. Haarer, *Nature*, 1994, **371**, 141.
7 A. M. Craats, J. M. Warman, A. Fechtenkötter, J. D. Brand, M. A. Harbison and K. Müllen, *Adv. Mater.*, 1999, **11**, 1469.
8 L. Schmidt-Mende, A. Fechtenkotter, K. Müllen, E. Moons, R. H. Friend and J. D. MacKenzie, *Science*, 2001, **293**, 1119.
9 H. Gunther, C. Emma, B. Joaquin, G.-L. Berta, E. H. Robert, T. Mara, G. Attilio and L. S. Jose, *Chem. Mater.*, 2007, **19**, 6068.
10 Y. Xu, S. Leng, C. Xue, R. Sun, J. Pan, J. Ford and S. Jin, *Angew. Chem., Int. Ed.*, 2007, **46**, 3896.
11 S. Sergeyev, W. Pisulab and Y. H. Geerts, *Chem. Soc. Rev.*, 2007, **36**, 1902.
12 M. Kastler, W. Pisula, F. Laquai, A. Kumar, R. J. Davies, S. Baluschev, M.-C. Garcia-Gutiérrez, D. Wasserfallen, H.-J. Butt, C. Riekel, G. Wegner and K. Müllen, *Adv. Mater.*, 2006, **18**, 2255.
13 F. Gholamrezaie, S. G. J. Mathijssen, E. C. P. Smites, T. C. T. Genus, P. A. van Hal, S. A. Ponomarenko, H.-G. Flesch, R. Resel, E. Cantatore, P. W. M. Blom and D. M. de Leeuw, *Nano Lett.*, 2010, **10**, 1998.
14 J. M. Warman, M. P. de Haas, G. Dicker, G. C. Grozema, J. Piris and M. G. Debije, *Chem. Mater.*, 2004, **16**, 4600.
15 Y.-J. Bae, H.-J. Yang, S.-H. Shin, K.-U. Jeong and M.-H. Lee, *J. Mater. Chem.*, 2011, **21**, 2074.
16 L. Wang, H. Cho, S.-H. Lee, C. Lee, K.-U. Jeong and M.-H. Lee, *J. Mater. Chem.*, 2011, **21**, 60.
17 H. J. Choi, K.-U. Jeong, L.-C. Chien and M.-H. Lee, *J. Mater. Chem.*, 2009, **19**, 7124.
18 H. Hoppe, D. A. M. Egbe, D. Mühlbacher and N. S. Sariciftci, *J. Mater. Chem.*, 2004, **14**, 3462.
19 S. Zimmermann, J. H. Wendorff and C. Weder, *Chem. Mater.*, 2002, **14**, 2218.
20 M. Yoshio, T. Kagata, K. Hoshino, T. Mukai, H. Ohno and T. Kato, *J. Am. Chem. Soc.*, 2006, **128**, 5570.
21 K. L. Woon, M. P. Aldred, P. Vlachos, G. H. Mehl, T. Stirner, S. M. Kelly and M. O'Neill, *Chem. Mater.*, 2006, **18**, 2311.
22 M. Funahashi, F. Zhang and N. Tamaoki, *Adv. Mater.*, 2007, **19**, 353.
23 A. El-Ghayoury, L. Douce, A. Skoulios and R. Ziessel, *Angew. Chem., Int. Ed.*, 1998, **37**, 1255.
24 S. Mery, D. Haristoy, J.-F. Nicoud, D. Guillon, S. Diele, H. Monobe and Y. Shimizu, *J. Mater. Chem.*, 2002, **12**, 37.

25 A. Mori, M. Yokoo, M. Hashimoto, S. Ujiie, S. Diele, U. Baumeister and C. Tschierske, *J. Am. Chem. Soc.*, 2003, **125**, 6620.
26 T. Cardinaels, K. Driesen, T. N. Parac-Vogt, B. Heinrich, C. Bourgogne, D. Guillon, B. Donnio and K. Binnemans, *Chem. Mater.*, 2005, **17**, 6589.
27 S. Norvez, F.-G. Tournilhac, P. Bassoul and P. Herson, *Chem. Mater.*, 2001, **13**, 2552.
28 L. Cui and L. Zhu, *Langmuir*, 2006, **22**, 5982.
29 L. Cui, J. Miao and L. Zhu, *Macromolecules*, 2006, **39**, 2536.
30 R. A. Bissell, N. Boden, R. J. Bushby, C. W. G. Fishwick, E. Holland, B. Movaghar and G. Ungar, *Chem. Commun.*, 1998, 113.
31 J. L. Segura and N. Martin, *Angew. Chem., Int. Ed.*, 2001, **40**, 1372.
32 A. B. Braunschweig, B. H. Northrop and J. F. Stoddart, *J. Mater. Chem.*, 2006, **16**, 32.
33 N. Martin, L. Sanchez, M. A. Herranz, B. Illescas and D. M. Guldi, *Acc. Chem. Res.*, 2007, **40**, 1015.
34 J. Liao, J. S. Agustsson, S. Wu, C. Schönenberger, M. Calame, Y. Leroux, M. Mayor, O. Jeannin, Y.-F. Ran, S.-X. Liu and S. Decurtins, *Nano Lett.*, 2010, **10**, 759.
35 L. Wang, K.-U. Jeong and M.-H. Lee, *J. Mater. Chem.*, 2008, **18**, 2657.
36 N. B. Chanh, M. Cotrait, J. Gautlier, Y. Haget, H. T. Nguyen, C. Polycarpe and E. Torreilles, *Mol. Cryst. Liq. Cryst.*, 1983, **101**, 129.
37 R. A. Bissell, N. Boden, R. J. Bushby, C. W. G. Fishwick, E. Holland, B. Movaghar and G. Ungar, *Chem. Commun.*, 1998, 113.
38 E. Allard, F. Oswald, B. Donnio, D. Guillon, J. L. Delgado, F. Langa and R. Deschenaux, *Org. Lett.*, 2005, **7**, 383.
39 I. C. Pintre, J. L. Serrano, M. B. Ros, J. Ortega, I. Alonso, J. Martinez-Perdiguero, C. L. Folcia, J. Etxebarria, F. Goc, D. B. Amabilino, J. Puigmarti-Luis and E. Gomar-Nadal, *Chem. Commun.*, 2008, 2523.
40 T. Yasuda, K. Tanabe, T. Tsuji, K. K. Coti, I. Aprahamian, J. F. Stoddart and T. Kato, *Chem. Commun.*, 2010, **46**, 2523.
41 Y.-L. Zhao, N. Erina, T. Yasuda, T. Kato and J. F. Stoddart, *J. Mater. Chem.*, 2009, **19**, 3469.
42 C. Rovira, *Angew. Chem., Int. Ed.*, 2006, **45**, 3003.
43 L. Wang, S.-J. Park, S.-H. Lee, Y.-J. Kim, Y.-B. Kook, S.-W. Kuo, R. M. van Horn, S. Z. D. Cheng, M.-H. Lee and K.-U. Jeong, *Chem. Mater.*, 2009, **21**, 3838.
44 A. Coskun, P. J. Wesson, R. Klajn, A. Trabolsi, L. Fang, M. A. Olson, S. K. Dey, B. A. Grzybowski and J. F. Stoddart, *J. Am. Chem. Soc.*, 2010, **132**, 4310.
45 K.-U. Jeong, B. S. Knapp, J. J. Ge, S. Jin, M. J. Graham, H. Xiong, F. W. Harris and S. Z. D. Cheng, *Macromolecules*, 2005, **38**, 8333.
46 K.-U. Jeong, B. S. Knapp, J. J. Ge, M. J. Graham, Y. Tu, S. Leng, H. Xiong, F. W. Harris and S. Z. D. Cheng, *Polymer*, 2006, **47**, 3351.
47 K.-U. Jeong, B. S. Knapp, J. J. Ge, S. Jin, M. J. Graham, F. W. Harris and S. Z. D. Cheng, *Chem. Mater.*, 2006, **18**, 680.
48 I. Nishiyama, J. Yamamoto, J. W. Goodby and H. Yokoyama, *J. Mater. Chem.*, 2001, **11**, 2690.
49 K.-U. Jeong, D. K. Yang, M. J. Graham, Y. Tu, S.-W. Kuo, B. S. Knapp, F. W. Harris and S. Z. D. Cheng, *Adv. Mater.*, 2006, **18**, 3229.
50 K.-U. Jeong, A. J. Jing, B. Monsdorf, M. J. Graham, F. W. Harris and S. Z. D. Cheng, *J. Phys. Chem. B*, 2007, **111**, 767.
51 S. Z. D. Cheng, in *Phase Transitions in Polymers*, Elsevier, New York, 2008.
52 I. Dierking, in *Textures of Liquid Crystals*, Wiley-VCH, Weinheim, 2003.
53 J. Cheng, Y. Jin, B. Wunderlich, S. Z. D. Cheng, M. A. Yandrasits, A. Zhang and V. Percec, *Macromolecules*, 1992, **25**, 5991.
54 D. McElheny, J. Grinshtein, V. Frydman and L. Frydman, *Macromolecules*, 2002, **35**, 3544.
55 H. Ishida and F. Horii, *Macromolecules*, 2002, **35**, 5550.
56 C. Xue, S. Jin, X. Weng, J. J. Ge, Z. Shen, H. Shen, M. J. Graham, K.-U. Jeong, H. Huang, D. Zhang, M. Guo, F. W. Harris, S. Z. D. Cheng, C. Y. Li and L. Zhu, *Chem. Mater.*, 2004, **16**, 1014.
57 H. Shen, K.-U. Jeong, H. Xiong, M. J. Graham, S. Leng, J. X. Zheng, H. Huang, M. Guo, F. W. Harris and S. Z. D. Cheng, *Soft Matter*, 2006, **2**, 232.
58 L. D. Gaetani and G. Prampolini, *Soft Matter*, 2009, **5**, 3517.
59 C. V. Yelamaggad, G. Shanker, U. S. Hiremath and S. K. Prasad, *J. Mater. Chem.*, 2008, **18**, 2927.